# Time-dependent response of the overturning circulation and pycnocline depth to Southern Ocean surface wind stress changes MERICAN SOCIETY 1919

Hailu Kong<sup>a</sup> and Malte F. Jansen,<sup>b</sup>

<sup>a</sup> American Express Company, New York, New York

<sup>b</sup> Department of the Geophysical Sciences, The University of Chicago, Chicago, Illinois

Corresponding author: Hailu Kong, hlkong.uchicago@gmail.com

1

**Early Online Release:** This preliminary version has been accepted for publication in *Journal of Physical Oceanography* be fully cited, and has been assigned DOI 10.1175/JPO-D-21-0214.1. The final typeset copyedited article will replace the EOR at the above DOI when it is published.

ABSTRACT: Changes in the Southern Ocean (SO) surface wind stress influence both the meridional overturning circulation (MOC) and stratification not only in the SO but in the global oceans, which can take multiple millennia to fully equilibrate. We use a hierarchy of models to investigate the time-dependent response of the MOC and low-latitude pycnocline depth (which quantifies the stratification) to SO wind stress changes: a two-layer analytical theory, a multi-column model (PyMOC), and an idealized general circulation model (GCM). We find that in both the GCM and PyMOC, the MOC has a multi-decadal adjustment timescale while the pycnocline depth has a multi-centennial timescale. The two-layer theory instead predicts the MOC and pycnocline depth to adjust on the same, multi-decadal timescale. We argue that this discrepancy arises because the pycnocline depth depends on the bulk stratification, while the MOC amplitude is sensitive mostly to isopycnals within the overturning cell. We can reconcile the discrepancy by interpreting the "pycnocline depth" in the theory as the depth of a specific isopycnal near the maximum of the MOC. We also find that SO stationary eddies respond very quickly to a sudden wind stress change, compensating for most of the change in the Ekman-driven MOC. This effect is missing in the theory, where the eddy-induced MOC only follows the adjustment of the pycnocline depth. Our results emphasize the importance of depth-dependence in the oceans' transient response to changes in surface boundary conditions, and the distinct role played by stationary eddies in the SO.

SIGNIFICANCE STATEMENT: Our work resolves the question of why previous theories predict the ocean density structure to adjust to a change in the winds over the Southern Ocean within centuries, while climate models indicate that this adjustment takes thousands of years. The question is important because it is related to our understanding of how the ocean responds to potential climate change scenarios. Our results emphasize the importance of depth-dependence in the density response (i.e., the upper ocean adjusts faster than the deep ocean), suggesting that future theoretical advancement should be made with careful considerations of the ocean's vertical structure. Our results also highlight the role of stationary meanders in the Southern Ocean's Antarctic Circumpolar Current, whose influence has not been included in the existing theories.

## 1. Introduction

Surface westerlies over the Southern Ocean (SO) play a central role in driving the global ocean circulation, in part by pumping deep water to the surface and closing the global meridional overturning circulation (MOC; Toggweiler and Samuels 1995; Marshall and Radko 2003; Marshall and Speer 2012). The MOC is moreover closely linked to the ocean stratification at low latitudes, which affects not only the isopycnal slope in the SO, but diffusive upwelling in the basins and North Atlantic deep water (NADW) formation (e.g., Gnanadesikan 1999; Fürst and Levermann 2012).

Various theories have been proposed to understand the mechanisms controlling the MOC and stratification, and their response to SO wind stress changes (e.g., Gnanadesikan 1999; Wolfe and Cessi 2011; Sévellec and Fedorov 2011; Nikurashin and Vallis 2011, 2012; Shakespeare and Hogg 2012). Notably, Gnanadesikan (1999, hereafter G99) proposes an elegant two-layer theory for the MOC and stratification, where the latter is characterized by a single pycnocline depth. The theory shows that an increased SO wind stress has to be balanced by a deepened pycnocline and strengthened MOC. Nikurashin and Vallis (2012) generalize the theory by allowing for continuous vertical stratification. They show that both the magnitude and depth of the MOC significantly increase with the SO wind stress if the wind stress is close to the current climate. Both of these theories find an approximately 50% increase in the Atlantic meridional overturning circulation (AMOC) per doubling of the SO wind stress near the present climate. By comparison, Sévellec and Fedorov (2011) find the AMOC to increase by about 25% per doubling of the SO wind stress near current climate using a zonally averaged model, perhaps due to their use of a larger diapycnal

diffusivity than in the other two papers. Despite the quantitative differences, all these theories suggest that the SO wind stress significantly influences the AMOC.

Idealized global-scale general circulation models (GCM) have been used to test the theories and yield broadly consistent results (e.g., Nikurashin and Vallis 2012). However, both the theories and idealized GCM studies only incorporate crude representations of meso-scale eddies and standing meanders, which play crucial roles in the Southern Ocean MOC (SOMOC) and pycnocline depth (e.g., Gnanadesikan 1999; Hallberg and Gnanadesikan 2006; Thompson and Naveira Garabato 2014; Kong and Jansen 2021).

Idealized GCMs configured at eddy-permitting resolutions have thus been designed to specifically study the response of the SOMOC to SO wind stress changes. These studies have generally found that the SOMOC responds relatively weakly to wind stress changes, due to both transient and stationary eddies, which largely compensate for the change in the Ekman transport (Hallberg and Gnanadesikan 2006; Viebahn and Eden 2010; Abernathey et al. 2011; Morrison and Hogg 2013; Kong and Jansen 2021). However, the domains of the idealized GCMs used in these studies have a truncated meridional extent (as necessary due to computational limitations), making them unsuitable to investigate how the Southern Ocean circulation interacts with the AMOC and the global pycnocline depth. A relatively weak SOMOC response is also found in the eddy-permitting simulations of Munday et al. (2013), who use an idealized GCM that includes an inter-hemispheric basin that spans 60°S to 60°N, and limit (the still substantial) computational cost by choosing a domain that is only 20° wide longitudinally. This allows for an explicit representation of NADW formation, although the width of the domain does affect the strength and depth of the AMOC (e.g., Nadeau and Jansen 2020).

More complex GCMs with realistic continental configuration have also been used to investigate the response of the MOC to SO wind stress changes. Again, the SOMOC is found to respond less strongly than expected from purely Ekman-driven theory, consistent with the aforementioned idealized GCM studies (Farneti and Delworth 2010). The AMOC is also found to increase with the wind stress on multi-decadal timescales (Delworth and Zeng 2008; Klinger and Cruz 2009; Ma et al. 2010; Farneti and Delworth 2010; Wei et al. 2012). However, due to computational limitations, none of these simulations have reached full equilibrium, making their results not readily comparable to the theories and idealized modeling studies, which generally consider the

equilibrium responses. Previous studies have found that the transient and equilibrium responses of the MOC to changes in other types of boundary conditions, such as surface buoyancy, can differ qualitatively (e.g., Jansen et al. 2018).

While much theoretical progress has been made to understand the equilibrium response of the global ocean circulation to SO wind stress changes, less work has focused on the theoretical understanding of the time-dependent response. A first step in this direction has been taken by Jones et al. (2011, hereafter J11), Allison et al. (2011), and Samelson (2011), who essentially extend the two-layer theory of G99 to include time-dependence in the global pycnocline depth. These theories all predict a multi-decadal to centennial e-folding adjustment timescale for the pycnocline depth<sup>1</sup>, which, however, is significantly shorter than the multi-centennial timescale found in the GCM simulations of J11.

In the present work we use a hierarchy of models to investigate the time-dependent (both transient and equilibrium) response of the MOC and pycnocline depth to changes in SO surface wind stress. Using an idealized GCM with a sophisticated state-of-the-art eddy parameterization, we show that the MOC adjusts on a multi-decadal timescale, while the pycnocline depth, as defined by G99, needs multiple millennia to fully equilibrate. The time-dependent two-layer theory of J11 cannot capture the disparate timescales, as the MOC in the theory is by construction linked to the pycnocline depth, which represents the only prognostic variable in the model. We argue that the main limitation of the theory is that the deep ocean stratification and its adjustment cannot be adequately captured by a single pycnocline depth. In addition, the theory cannot adequately capture the effect of standing meanders in the SO, which are directly sensitive to the wind stress changes, rather than depending only on the zonal mean isopycnal slopes (and hence pycnocline depth), as assumed in the SO eddy parameterization applied in the theory. Our conclusions are corroborated by a multicolumn model for the MOC (Jansen and Nadeau 2019, hereafter JN19), which fully resolves the vertical stratification and parameterizes the effect of stationary eddies.

# 2. Model hierarchy

We adopt a hierarchy of models to decipher the mechanisms that control the time-dependent response of the MOC and pycnocline depth to SO wind stress changes. Specifically, we consider

<sup>&</sup>lt;sup>1</sup>For Allison et al. (2011), we are referring to their version of the theory that includes NADW formation, which significantly reduces the adjustment timescale.

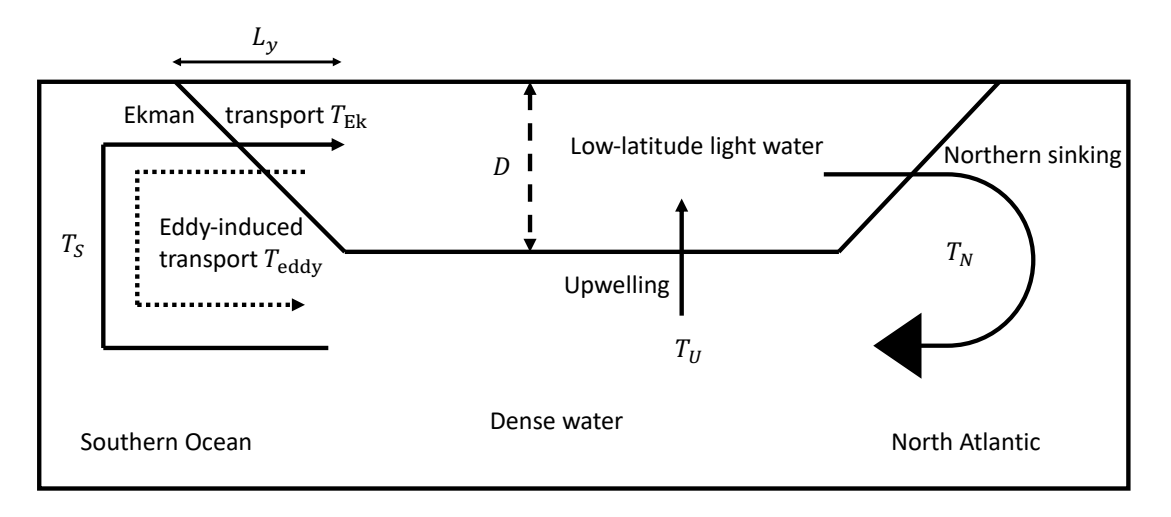


Fig. 1. A schematic of the two-layer model by G99 (adapted from G99).

a two-layer analytical box model (G99, J11), a multicolumn toy model (based on JN19), and an idealized GCM serving as the benchmark. The complexity of ocean dynamics increases with the model hierarchy, with which we aim to identify and understand the key elements affecting the deep ocean response to SO wind changes.

## a. Equilibrium theory

In this section we review the two-layer analytical box model of G99, which focuses on the equilibrium relation between the MOC and pycnocline depth. The two-layer model assumes that the northern sinking caused by deep convection,  $T_N$ , is balanced by the upwelling in the low latitudes,  $T_U$ , and in the SO,  $T_S$  (Fig. 1):

$$0 = T_S + T_{IJ} - T_N. \tag{1}$$

The SO component can be further decomposed as

$$T_S = T_{\rm Ek} - T_{\rm eddv},\tag{2}$$

where

$$T_{\rm Ek} = \frac{\tau}{\rho |f|} L_x \tag{3}$$

is the wind-driven SOMOC, given by the Ekman transport. Here  $\tau$  is the mean wind stress over the SO, computed using the wind stress profile in the GCM (see section 2d) averaged between 65°S to 30°S,  $L_x$  is the zonal extent of the ACC,  $\rho$  the density, and f the Coriolis parameter.  $T_{\rm eddy}$  is the eddy-induced overturning, which is parameterized as

$$T_{\text{eddy}} = K \frac{D}{L_{y}} L_{x},\tag{4}$$

where D is the pycnocline depth,  $L_y$  the meridional extent of the ACC, and K the Gent and McWilliams (1990, hereafter GM) eddy diffusivity. In the original paper of G99, K takes a constant value. In J11, it is further parameterized to depend on the pycnocline depth D as

$$K = K_0 \left(\frac{D}{D_0}\right)^{n-1},\tag{5}$$

where  $K_0$  is a reference diffusivity,  $D_0$  a reference pycnocline depth, and n a positive integer. When n = 1 we retrieve the original formulation in G99; increasing the value of n increases the sensitivity of the eddy diffusivity to the isopycnal slope. In the present work, we consider the cases of n = 3 and n = 8, where n = 3 is most consistent with the sensitivity of the GM diffusivity to the isopycnal slope in the parameterization used in the GCM (see section 2d and Appendix A for more details), while n = 8 yields a solution that empirically compares more favorably with the GCM results and is also the largest value of n considered in J11.

The low-latitude diapycnal upwelling  $T_U$  is determined by the balance between downward buoyancy diffusion and upward water mass advection, yielding

$$T_U = \frac{\kappa_d A}{D},\tag{6}$$

where  $\kappa_d$  is the diapycnal diffusivity and A the area of upwelling.

The northern sinking is assumed to take the form of

$$T_N = \frac{cg'}{f}D^2,\tag{7}$$

TABLE 1. Values of parameters used in our solution of the two-layer model. The parameters are chosen to match the idealized GCM simulations described in section 2d.

Parameter	Value	Parameter	Value
$L_x$	5000 km	$L_{\rm y}$	2000 km
ho	$1030 \text{ kg m}^{-3}$	f	$1 \times 10^{-4} \text{s}^{-1}$
$K_0$	$1349 \text{ m}^2 \text{ s}^{-1}$	$D_0$	741 m
$\kappa_d$	$5 \times 10^{-5} \text{ m}^2 \text{s}^{-1}$	A	$6 \times 10^{13} \text{ m}^2$
g'	$0.01 \text{ m s}^{-2}$	c	0.15

where c is a constant of proportionality and g' the reduced gravity. Notice that Eq. (7) differs from the formulation in G99 by replacing  $\beta L_y$  with f, where  $\beta$  is the meridional gradient of the Coriolis parameter and  $L_y$  the meridional extent across which the pycnocline shoals in the northern hemisphere. Eq. (7) arises from the thermal wind relation and assumes that the northern sinking can be related to a zonal geostrophic transport in the north of the basin, following Nikurashin and Vallis (2012). Practically, Eq. (7) is equivalent to the original formulation in G99, who assumes a viscous boundary current scaling, as long as the parameter c is retuned accordingly.

By substituting Eqs. (2)-(7) into Eq. (1) we can solve for the equilibrium value of the pycnocline depth,  $D_{eq}$ , which then allows us to infer all transports from Eqs. (2)-(7). The values of the model parameters are summarized in Table 1, and the procedure that was used to tune these parameters is documented in Appendix A.

## b. Transient adjustment

Several theories have been proposed to predict the adjustment timescale of the pycnocline depth and MOC (J11; Allison et al. 2011; Samelson 2011). Here we follow the formulation of J11, but we note that all three papers suggest essentially the same scaling relation.

J11 generalizes the two-layer theory of G99 by including a tendency term on the L.H.S. of Eq. (1), such that

$$A\frac{\mathrm{d}D}{\mathrm{dt}} = T_S + T_U - T_N. \tag{8}$$

Linearizing Eq. (8) about the equilibrium solution at wind stress  $\tau$ , such that  $D(t) = D_{\rm eq} + \Delta D(t)$  (where the subscript "eq" denotes the equilibrium solution) with  $|\Delta D(t)| \ll |D_{\rm eq}|$ , we obtain an

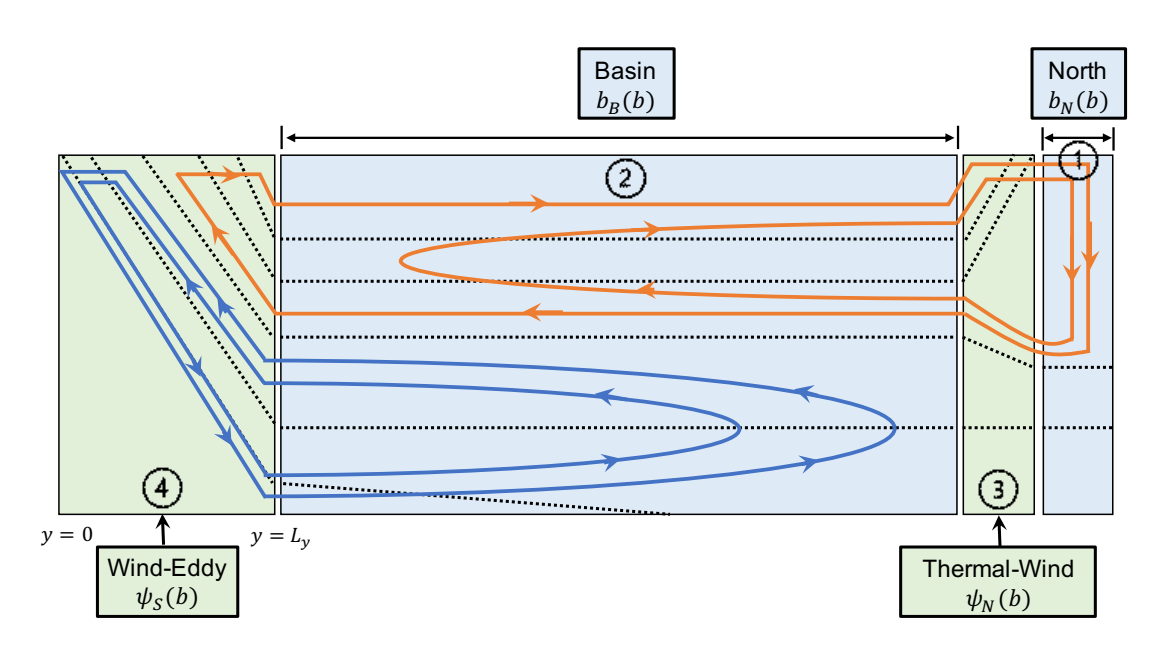


Fig. 2. A schematic of our PyMOC model setup (based on JN19).

exponential decay of the anomaly,  $\Delta D(t)$ , with an e-folding timescale:

$$t_0 = \frac{AD_{\text{eq}}}{T_{\text{U,eq}} + 2T_{\text{N,eq}} + nT_{\text{eddy,eq}}}.$$
(9)

Readers are referred to Appendix B for the derivation of Eq. (9).

All components of the MOC, except the Ekman-driven MOC, are related to the pycnocline depth via the diagnostic relations introduced in section 2a. For relatively small amplitude perturbations to the pycnocline depth, the theory therefore implies that all components of the circulation, except the Ekman-driven MOC, adjust with approximately the same timescale.

# c. PyMOC: A multicolumn model for the MOC

We use a modified version of the multicolumn model introduced in JN19 (named "PyMOC") as the intermediate complexity model among the model hierarchy. PyMOC is essentially a multi-layer generalization of the box model introduced above, and therefore has the ability to resolve depth-dependent changes in the circulation and stratification. Readers are referred to JN19 for details of the model, which we here review only briefly, while highlighting our modifications in particular to the formulation of the eddy-induced MOC in the SO.

In PyMOC, predictive equations for the buoyancy are solved in two regions, the northern sinking region and the interior basin, denoted as 1 and 2 in Fig. 2, respectively:

$$\partial_t b = -w^{\dagger} \partial_z b + \partial_z (\kappa_d \partial_z b), \tag{10}$$

where b is the buoyancy,  $w^{\dagger}$  the residual upwelling, and  $\kappa_d$  the diapycnal diffusivity. A convective adjustment is included in the northern column (region 1 in Fig. 2), which restores the stratification to a minimal value of  $1\times10^{-7}$  s<sup>-2</sup>.

The overturning circulation between the northern sinking region and the basin (region 3 of Fig. 2) is computed via the thermal wind relation, following Nikurashin and Vallis (2012):

$$\partial_{zz}\psi_N(z) = -f^{-1}[b_B(z) - b_N(z)],\tag{11}$$

where  $b_B$  and  $b_N$  are the buoyancy in the basin and the northern sinking region, respectively. The streamfunction  $\psi_N$  is mapped into buoyancy coordinates using the upstream buoyancy profile (i.e.,  $b_B$  if the flow is northward at a given depth and  $b_N$  if it is southward) and, together with the circulation in the SO, is used to compute the residual vertical velocity  $w^{\dagger}$  in Eq. (10).

Unlike in JN19, the SO surface buoyancy profile (the surface of region 4 in Fig. 2) is here prescribed as a linear function of latitude, similar to Kong and Jansen (2021). Specifically, the profile  $b_S$  is

$$b_S(y) = b_0 y / L_y, \tag{12}$$

where  $b_0$  is the surface buoyancy in the basin,  $0 \le y \le L_y$  is the meridional coordinate in the SO, and  $L_y$  the width of the SO. A fixed linear profile for the surface buoyancy is broadly consistent with the idealized GCM simulations that will be discussed in section 2d, whose surface buoyancy is rapidly restored towards a linear profile.

The SOMOC streamfunction,  $\psi_S$ , in PyMOC (region 4 in Fig. 2) follows Marshall and Radko (2003) (cf. Marshall and Zanna 2014):

$$\psi_S(b) = \psi_{Ek}(b) + \psi_{eddy}(b) = \frac{\overline{\tau(b)}L_x}{\rho|f|} + L_x K_{eff} s(b), \tag{13}$$

where  $\psi_{Ek}$  and  $\psi_{eddy}$  are the Ekman-driven and eddy-induced MOC, respectively;  $K_{eff}$  is the effective eddy diffusivity, s the isopycnal slope, and  $\overline{\tau(b)}$  the averaged surface wind stress over the latitudinal range of the isopycnal with buoyancy b:

$$\overline{\tau(b)} = \frac{1}{L_y - L(b)} \int_{L(b)}^{L_y} \tau(y) \, dy,$$
 (14)

where L(b) is the outcropping location of the isopycnal with buoyancy b. Instead of a spatially constant  $\tau$  (as used in JN19), we use a meridional sinusoidal profile for the wind stress, which crudely approximates the present climate and the wind stress profile in the GCM introduced in section 2d:

$$\tau(y) = \tau_0 \sin(\pi y / L_y),\tag{15}$$

where  $\tau_0$  is the peak wind stress.

The effective eddy diffusivity,  $K_{\text{eff}}$ , which is meant to capture the effect of both transient and stationary eddies, is approximated as the product of the transient diffusivity  $K_{\text{tr}}$  and a stretching factor that depends on the wind stress:

$$K_{\text{eff}} = K_{\text{tr}} \left( 1 + \alpha \frac{\tau_0}{\tau_{\text{ref}}} \right), \tag{16}$$

where  $\alpha$  is a non-dimensional constant,  $\tau_0$  the peak SO wind stress, and  $\tau_{ref}$  the peak wind stress in the reference case, which corresponds to the present climate.

The transient eddy diffusivity is

$$K_{\rm tr} = K_1 \left(\frac{D}{D_0}\right)^{n-1},\tag{17}$$

where  $K_1$  is the transient diffusivity in the reference climate.  $K_1$  depends on the (zonally averaged) isopycnal slope, as transient eddies extract their energy from the available potential energy (APE) of the mean flow via baroclinic instability, and we here use the generalized formulation proposed by J11. Note that Eq. (17) (as well as Eq. (5) used in the J11 model) assumes that the eddy diffusivity adjusts instantly to a change in the isopycnal slope, unlike in the eddy kinetic energy (EKE)-budget-based eddy parameterization that we use in the GCM (see section 2d below). This assumption is adequate on timescales much longer than the frictional damping timescale of the EKE. The frictional timescale is on the order of months (e.g., Sinha and Abernathey 2016; Mak

TABLE 2. Values of parameters used in our configuration of PyMOC and PyMOC-no-meander (shown in parentheses where they differ from PyMOC).  $b_n$  is the surface buoyancy in the NADW formation region. Other parameters are defined in the text. Additional parameters are identical to those listed in table 1 for the two-layer theory.

Parameter	Value	Parameter	Value
$K_1$	710 (1349) $m^2 s^{-1}$	n	3 (8)
$\alpha$	0.9(0)	$b_0$	$0.018~{\rm ms^{-2}}$
$ au_{ ext{ref}}$	0.2 Pa	$b_n$	$0.004~{\rm ms^{-2}}$
$D_0$	788 m		

et al. 2018), and thus much shorter than the multi-decadal to millennial timescales of global pycnocline and MOC adjustment that are the focus of this study. However, the EKE adjustment is expected to lead to interesting modifications of the SO response to wind-fluctuations on much shorter timescales (cf. Sinha and Abernathey 2016).

Stationary eddies enhance the effect of transient eddies by elongating the contours of buoyancy and sharpening the cross-contour gradients (Nakamura 1996, 2001; Abernathey and Cessi 2014; Kong and Jansen 2021). In Eq. (16) this enhancement is quantified by the stretching factor  $K_{\rm eff}/K_{\rm tr}$ , which we assume to take the form of  $1 + \alpha \tau_0/\tau_{\rm ref}$ . This simple linear dependence on the wind stress is crudely based on the diagnosis in Kong and Jansen (2021, Appendix C). We assume that this stretching factor adjusts instantly to a wind stress change, because the standing eddies are expected to respond to a wind stress change within months (e.g., Wearn and Baker 1980). A fast adjustment of the standing eddy contribution has also been confirmed for the idealized GCM simulations in the present study (not shown). Notice that  $K_{\rm tr}$  itself can also depend on the fast response of the meanders, which sharpen the local buoyancy gradients. An attempt to explicitly include this effect in our parameterization, however, did not significantly affect our results, and we therefore here focus on the simpler formulation in Eq. (17). For consistency with the GCM simulations (see section 2d), we choose n = 3, while  $K_1$ ,  $D_0$ , and  $\alpha$  have been tuned to reproduce the diagnosed effective diffusivity from the GCM simulations (see Appendix A for additional details) and are given in Table 2 together with additional PyMOC parameters.

To isolate the distinct role of parameterized standing meanders in Eq. (16), we have also configured a second version of PyMOC, here called PyMOC-no-meander, which is almost identical

to PyMOC except that it does not include an explicit representation of the impact of wind stress changes on standing meanders. Specifically, it uses (a)  $\alpha = 0$  with a re-tuned value of  $K_1$  to reproduce the reference climate (see table 2), and (b) n = 8, instead of 3, to reproduce the same wind stress sensitivity by increasing the sensitivity to the pycnocline depth instead of including a direct wind stress dependence. As will be shown below, this approach can capture the equilibrium sensitivity of the pycnocline depth and MOC equally well, but fails to reproduce the time-dependent response.

# d. An idealized GCM for the MOC

On the most complex end of our model hierarchy we use an idealized inter-hemispheric GCM (the "shoebox"; see Fig. 3) to study the time-dependent response of the MOC and pycnocline to changes in SO surface westerlies. The model uses MOM6 in a purely isopycnal configuration with potential density as the only state variable. The shoebox configuration extends the SO model introduced in Kong and Jansen (2021) to include a basin to the north of the SO. The shoebox is zonally reentrant at Drake Passage latitudes and otherwise is enclosed by boundaries with a continental slope. Apart from the slope, the only bottom topography is an idealized representation of Scotia Arc downstream of Drake Passage, which helps generate stationary meanders that are crucial for the Southern Ocean circulation (e.g., Thompson and Naveira Garabato 2014; Kong and Jansen 2021). The top of "Scotia Arc" is 2500m deep, fully blocking the f/h contours. The shoebox configuration essentially mimics the Atlantic basin and the SO at its south.

The GCM is forced at the surface by zonally symmetric eastward wind stress (Fig. 4(a)), and surface density is restored towards an idealized profile (Fig. 4(b)) with a piston velocity of 2 m day<sup>-1</sup>. The densest surface water in the northern hemisphere is slightly lighter than that in the southern hemisphere, to ensure that Antarctic Bottom Water (AABW) forms in the southern hemisphere.

The GCM is configured at 1° resolution and uses the Topographically modified Meso-scale Eddy Kinetic Energy parameterization (TMEKE; Jansen et al. 2015, 2019). The TMEKE parameterization predicts the evolution of vertically integrated sub-grid-scale EKE and uses it to formulate the GM diffusivity. The mixing length that enters the GM diffusivity is assumed to scale with a generalized Rhines scale, modified to include the effect of topography on the planetary potential

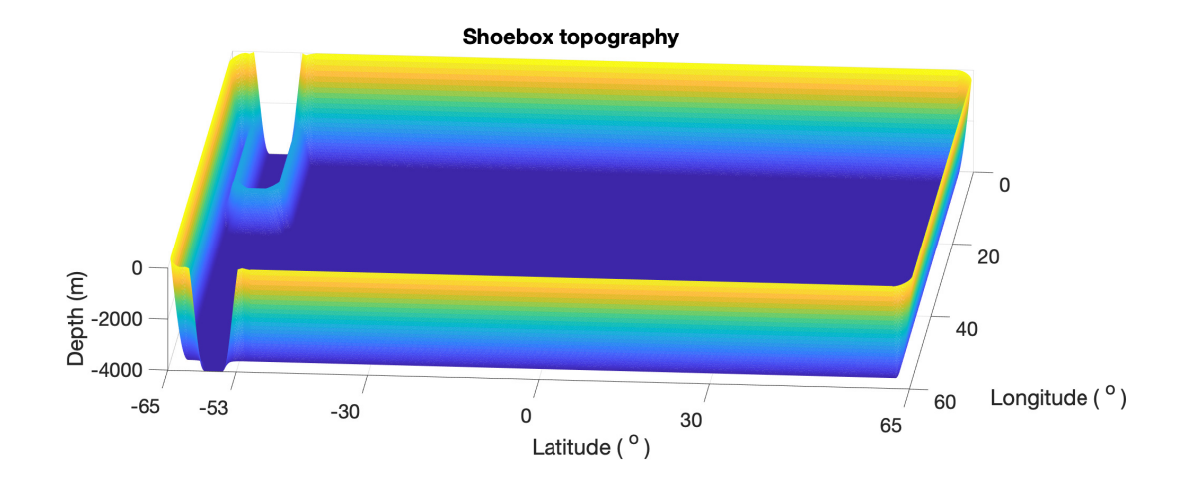


Fig. 3. 3D view of the bottom topography in the shoebox configuration of the GCM. Color shading denotes the depth.

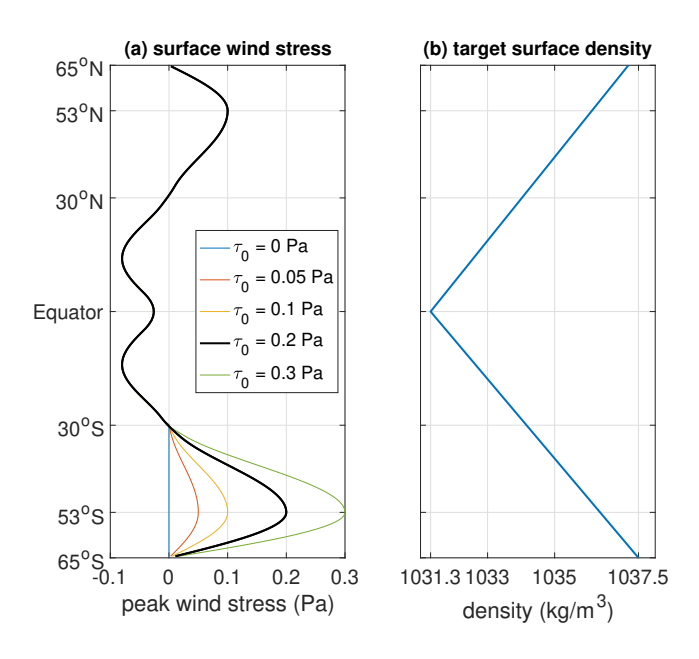


Fig. 4. (a) Surface zonal wind stress profile. Black curve denotes the reference case. All 5 cases share the same wind stress profile north of 30°S. (b) Target density profile for surface restoring.

vorticity gradient. The specific configuration follows Kong and Jansen (2021, Appendix A), except that an extra background diffusivity of 100 m<sup>2</sup>s<sup>-1</sup> has been added to reduce unrealistic variability in the basin. It has been shown in Kong and Jansen (2021) that simulations using the TMEKE parameterization at 1° resolution can accurately capture the SOMOC response to SO wind stress changes in the SO-only version of our model. We have also repeated most of our simulations using an eddy parameterization based on Visbeck et al. (1997), which yields broadly similar results (not

shown). Nevertheless, we note that the model's inability to explicitly resolve mesoscale eddies remains as a significant shortcoming, which is likely to have some effect on the quantitative results.

We analyze the model's response to a stepwise SO wind stress change in the following manner. The model is first forced with the reference wind stress profile in Fig. 4(a) (Southern Ocean peak wind stress  $\tau_0 = 0.2$  Pa) and integrated for 3600 years to reach statistical equilibrium. The SO wind stress profile is then changed abruptly in one timestep (colored curves in Fig. 4(a)) and the simulations are continued until a new equilibrium is obtained, which takes at least 3000 years. This step response experiment excites transient responses across the full spectrum of timescales that are represented by the model.

### 3. Results

## a. Reference state

The GCM captures the familiar 2D overturning structure under the reference wind stress profile (Fig. 5(b)), and the same circulation structure is qualitatively reproduced in PyMOC (Fig. 5(d)). Below the surface layer, two overturning cells can be discerned: an upper cell associated with NADW formation, and an abyssal cell associated with Antarctic bottom water formation. The vertical profiles of potential density are also qualitatively similar between the GCM and PyMOC. The northern density  $\sigma_N$  is approximately constant between about 500m and 1500m depth, consistent with the presence of convection and NADW formation, while the basin density  $\sigma_B$  follows approximately an exponential curve.

Some differences in the profiles of density and streamfunction between the GCM and PyMOC in the reference state are also noteworthy. Specifically, the GCM has a larger vertical density gradient near the surface than PyMOC (Fig. 5(a)(c)), because PyMOC cannot represent the ventilated thermocline in the upper ocean. Additionally, a strong negative isopycnal overturning exists around 40°S in the surface layer of the GCM (Fig. 5(a)), reflecting the gyre circulation that transports warm water poleward and cold water equatorward. The gyre circulation, by construction, is not included in PyMOC (Fig. 5(c)).

To quantify and compare the mean state and circulations across the 3 models, we focus on the following four variables:

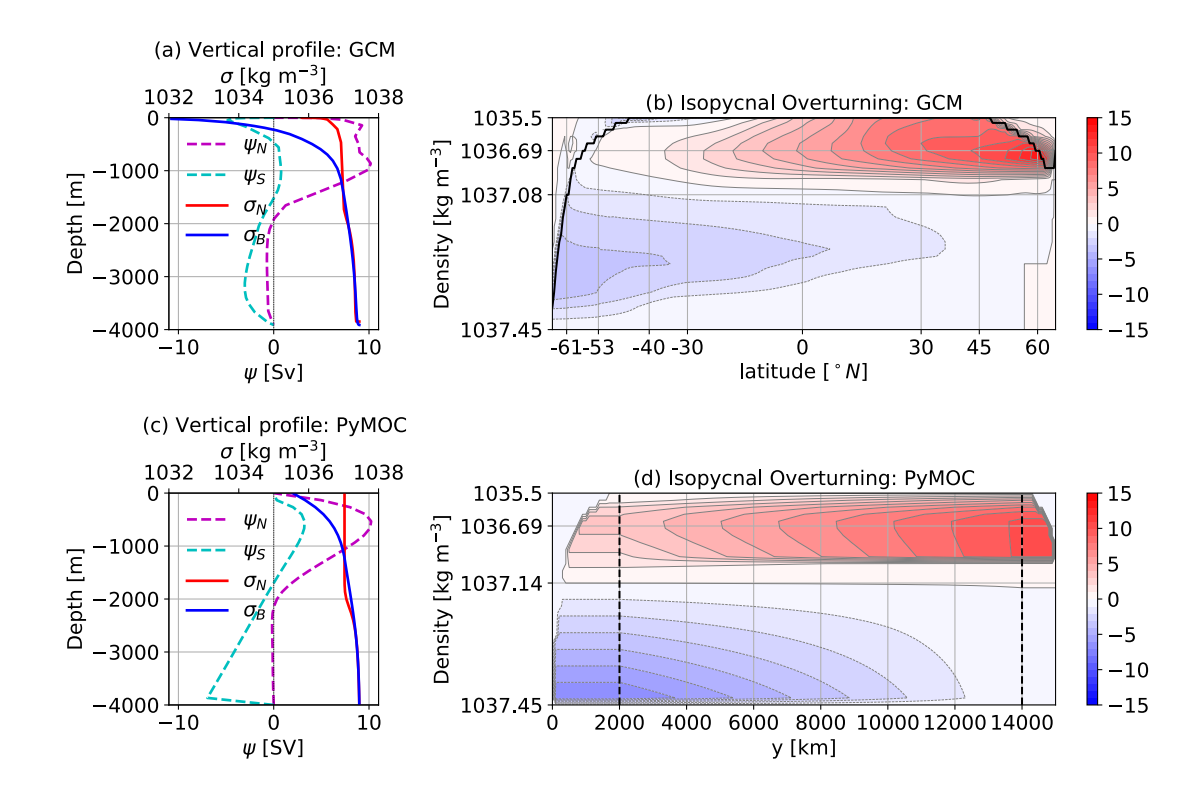


Fig. 5. Potential density and MOC in the reference simulation from the GCM (upper panel) and PyMOC (lower panel). (a) GCM results for the potential density profiles averaged over the basin between 40°S and 40°N ( $\sigma_B$ ) and in the NADW formation region between 61°N and 63°N ( $\sigma_N$ ), as well as the MOC profiles at 40°S ( $\psi_S$ ) and 45°N ( $\psi_N$ ), as functions of depth. The MOC profile in the GCM is mapped from density coordinates to depth coordinates according to the zonal mean depth of isopycnals at the respective latitudes. (b) Zonally integrated MOC from the GCM in isopycnal coordinates. The thick black curve denotes the bottom of the surface layer, and the horizontal density grid lines denote the center and bottom isopycnals of the AMOC at 45°N. (c) PyMOC solution of potential density profiles in the basin ( $\sigma_B$ ) and north ( $\sigma_N$ ), as well as the streamfunctions in the SO ( $\psi_S$ ) and north ( $\psi_N$ ). The potential density in PyMOC is computed as  $\sigma = \sigma_0(1 - bg^{-1})$ , where  $\sigma_0 = 1037.45$  kg m<sup>-3</sup> is an arbitrary reference density (chosen here such that the minimum potential density matches the GCM),  $\sigma_S$  the buoyancy, and  $\sigma_S$  the gravitational acceleration. (d) 2D interpolation of the streamfunction in PyMOC, assuming that the diapycnal upwelling is spatially homogeneous in the basin (bounded by vertical dashed lines). Surface density is linearly interpolated from the basin to the northern convective region. Notice that the density coordinates in (b) and (d) are not linear but stretched according to the density profile in the basin of PyMOC.

(1) the pycnocline depth D, defined following G99:

$$D = -\frac{\int_{z=-H}^{0} \Delta \sigma z dz}{\int_{z=-H}^{0} \Delta \sigma dz},$$
(18)

where H = 4000 m is the depth of the ocean and  $\Delta \sigma \equiv \sigma(z) - \sigma_{\text{max}}$ , with  $\sigma$  being the potential density (the only state variable in the GCM) and  $\sigma_{\text{max}}$  the domain-maximum potential density<sup>2</sup>. In the GCM, D is averaged between 40°S and 40°N, and excluding the 5° bordering the eastern & western boundaries, to avoid the impact of the continental slope. In PyMOC it is calculated using the buoyancy profile in the basin.

- (2) The AMOC ( $T_N$ ), defined as the maximum of the streamfunction at 45°N in the GCM, and as the maximum of the streamfunction between the basin and the NADW formation region in PyMOC.
- (3) The SOMOC ( $T_S$ ), defined as the maximum of the streamfunction at 40°S in the GCM (approximately the northernmost extent of the ACC meanders), and as the maximum of the streamfunction in the SO in PyMOC.
- (4) The low-latitude upwelling  $(T_U)$ , computed as  $T_N T_S^3$ .

Under the reference wind stress, the GCM results are broadly consistent with previous simulations and observations in these four variables (Fig. 6). Specifically, the GCM yields a pycnocline depth of 818 m, roughly similar to the GCM simulations discussed in G99 (~900 m). The AMOC and SOMOC in the GCM peak at 10.2 Sv and 0.78 Sv, respectively. The difference (9.4 Sv) is accounted for by the diapycnal upwelling in the basin. The AMOC, and in particular the SOMOC, are significantly weaker than in observations, which is expected based on the limited domain size (cf. Nadeau and Jansen 2020). In particular, the Southern Ocean is only 60° wide in our model. Multiplying the SOMOC transport by a factor of 6 to account for the zonal extend of the real Southern Ocean gives a more realistic SO overturning of 4.7 Sv [According to Lumpkin and Speer (2007), the upper cell transport is about 7 Sv at 40°S].

The two-layer theory roughly captures the pycnocline depth and the AMOC strength from the GCM simulation (partially as a result of how the parameters have been tuned - see Appendix A), but significantly overestimates the SOMOC and underestimates the upwelling in the basin. The SOMOC predicted by the theory is over 4 Sv, much larger than the 0.67 Sv transport in the GCM simulation. Conversely, the low-latitude upwelling predicted by the theory is only about 4 Sv, compared to 9.4 Sv in the GCM. The two-layer model cannot be tuned to reproduce all

<sup>&</sup>lt;sup>2</sup>Notice that the thus defined  $\sigma_{max}$  is insensitive to the wind stress changes and since it represents the maximum density of AABW, the resulting pycnocline depth is more representative of the isopycnal slopes in the SO than if  $\sigma_{max}$  is defined as the bottom density at each respective horizontal grid point. However, defining  $\sigma_{max}$  as the local bottom density would not alter our main conclusions here.

<sup>&</sup>lt;sup>3</sup>In both the GCM and PyMOC,  $T_N$  and  $T_S$  are evaluated on the isopycnal where the SOMOC and AMOC maximize (which in both models happens to be approximately the same isopycnal), so  $T_U$  represents the diapycnal upwelling across that isopycnal.

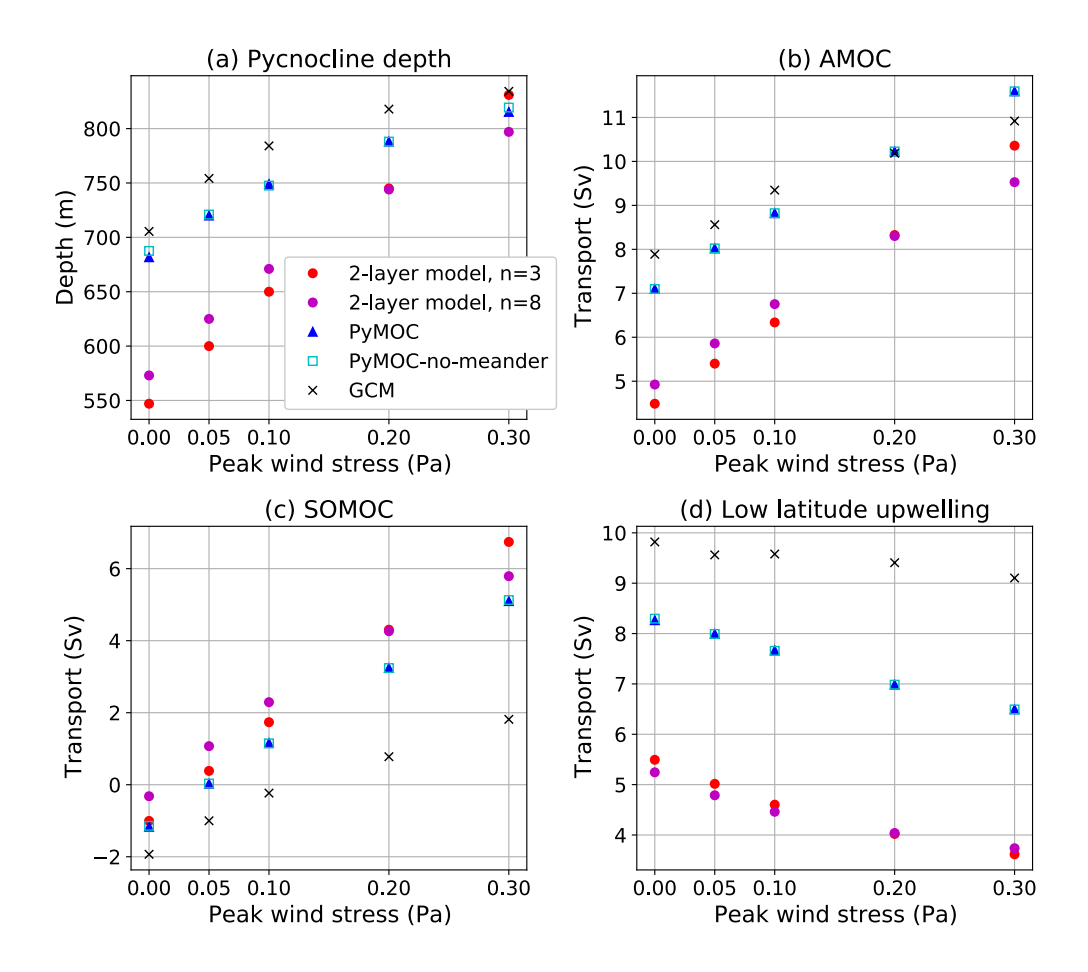


Fig. 6. Equilibrium solutions at varying wind stress for: (a) the pycnocline depth, (b) the AMOC, (c) the SOMOC, and (d) the low-latitude upwelling, from the two-layer theory, PyMOC, and the GCM (see legend in panel (a)).

four variables shown in Fig. 6, mainly because the scaling theory based on the advective-diffusive relation (Eq. (6)) does not predict the correct amount of upwelling given the correct pycnocline depth. The pycnocline depth as defined in Eq. (18) thus does not appear to be an accurate measure of the stratification scale that controls diapycnal upwelling in the GCM.

Both PyMOC and PyMOC-no-meander better capture the pycnocline depth, the SOMOC, and the upwelling, compared to the two-layer theory<sup>4</sup> (blue triangles and cyan squares in Fig. 6, respectively). This improvement is likely due to the multi-layer nature of PyMOC, where the MOC and upwelling are not assumed to be functions of a single depth scale. The PyMOC/PyMOC-no-meander solutions, however, still overestimate the SOMOC while underestimating the upwelling in the basin. Both of these inaccuracies may be caused by the simplified representation of the SO

<sup>&</sup>lt;sup>4</sup>Note that both PyMOC and PyMOC-no-meander are tuned to match the AMOC under the reference wind stress; see Appendix A.

overturning, which may not fully capture the impact of stationary eddies and geostrophic transport that plays an important role below and to the north of Drake Passage. Despite these shortcomings, both PyMOC and PyMOC-no-meander show clear improvement in representing the pycnocline depth, the MOC, and the upwelling under the reference wind stress, when compared to the two-layer theory.

# b. Equilibrium response to wind stress changes

In the GCM simulations, both the equilibrium pycnocline depth and MOC transport increase with the wind stress, while the low-latitude upwelling slightly decreases with wind stress (Fig. 6). The two-layer theory captures this qualitative response, but overestimates all sensitivities by approximately a factor of 2, depending on the value of n. The pycnocline depth in the GCM increases by about 129 m over the full wind stress range, compared to an increase of 284 m (n = 3) or 224 m (n = 8) in the theory. As a result, the theory predicts the AMOC to increase about 5.9 Sv (n = 3) or 4.6 Sv (n = 8), compared to an increase of only 3.0 Sv in the GCM. The SOMOC in the GCM increases by 3.7 Sv over the wind stress range, while the theory predicts an increase of 7.7 Sv (n = 3) or 6.1 Sv (n = 8). This overestimate of the SOMOC sensitivity can be related to an overall underestimate of the eddy-induced MOC,  $\psi_{\rm eddy}$ , whose relative sensitivity around the reference wind stress, defined here as  $\left(\psi_{\rm eddy}^{0.3 \, \rm Pa} - \psi_{\rm eddy}^{0.1 \, \rm Pa}\right)/\psi_{\rm eddy}^{0.2 \, \rm Pa}$  (where the superscript denotes the peak wind stress), is very close to that in the GCM: 0.72 (theory, n = 3) vs. 0.79 (GCM). Finally, in the GCM simulations, the upwelling only decreases by about 0.72 Sv over the wind stress range, compared to a decrease of 1.9 Sv (n = 3) or 1.5 Sv (n = 8) in the theory, which is related to the overestimated pycnocline depth sensitivity (via Eq. (6)).

PyMOC has a similarly sensitive pycnocline depth as the GCM while still overestimating the sensitivities of the MOC and upwelling (blue triangles in Fig. 6). As in the two-layer theory, the higher sensitivity of the SOMOC can be attributed to the overall weaker eddy-induced MOC, whose relative sensitivity is again very close to that in the GCM: 0.81 (PyMOC) vs. 0.79 (GCM). The SOMOC sensitivity in PyMOC-no-meander is similar to that in PyMOC, illustrating that the amplification of the effective diffusivity via the wind stress-dependent stretching term in PyMOC has a similar net effect on the equilibrium response as the much stronger pycnocline-depth sensitivity used in PyMOC-no-meander.

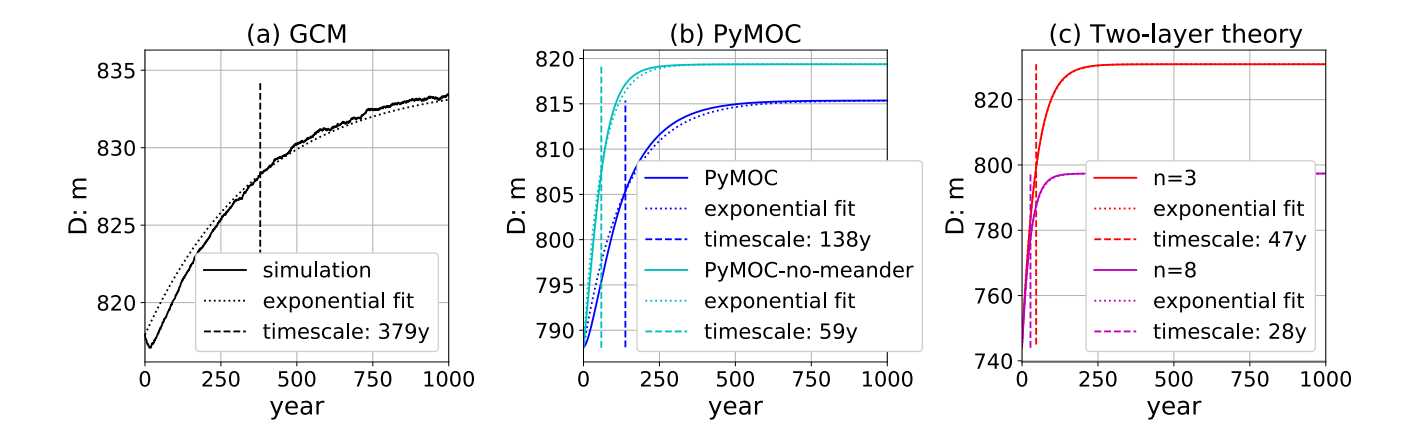


FIG. 7. Time-dependent response of the pycnocline depth to a wind stress increase from  $\tau_0 = 0.2$  Pa to 0.3 Pa, in: (a) the GCM; (b) PyMOC and PyMOC-no-meander; and (c) the two-layer theory, with n = 3 and n = 8. In all 3 panels, vertical dashed lines denote the corresponding e-folding adjustment timescales.

# c. Time-dependent response to wind stress changes

In this section we analyze the time-dependent response of the pycnocline depth and MOC to SO wind stress changes using our hierarchy of models.

### 1) Pycnocline depth

The pycnocline depth responds to an abrupt SO wind stress change approximately following an exponential curve with a multi-centennial adjustment timescale in the GCM simulations (Fig. 7(a)). For a wind stress increase from 0.2 Pa to 0.3 Pa (Fig. 7(a)), the e-folding timescale for the pycnocline depth is 379-years, although this timescale varies between 379 and 598 years, with longer adjustment timescales for wind stress reductions (not shown). Full equilibrium takes more than 1000 years to reach. PyMOC qualitatively captures the (multi-)centennial adjustment timescale (138 to 296 years), although the timescale is consistently shorter than in the GCM (Fig. 7(b)). This discrepancy may be partially due to the shallower pycnocline depth in PyMOC, compared to the GCM results under every wind stress considered (Fig. 6(a)), which results in a shorter theoretical timescale, according to Eq. (9). The discrepancy may further be amplified by the simple representation of SO eddies in PyMOC (Eqs. (16)(17)). Both PyMOC-no-meander and the two-layer theory have multi-decadal adjustment timescales, and are thus substantially underestimating the adjustment timescale (Fig. 7(b)(c)).

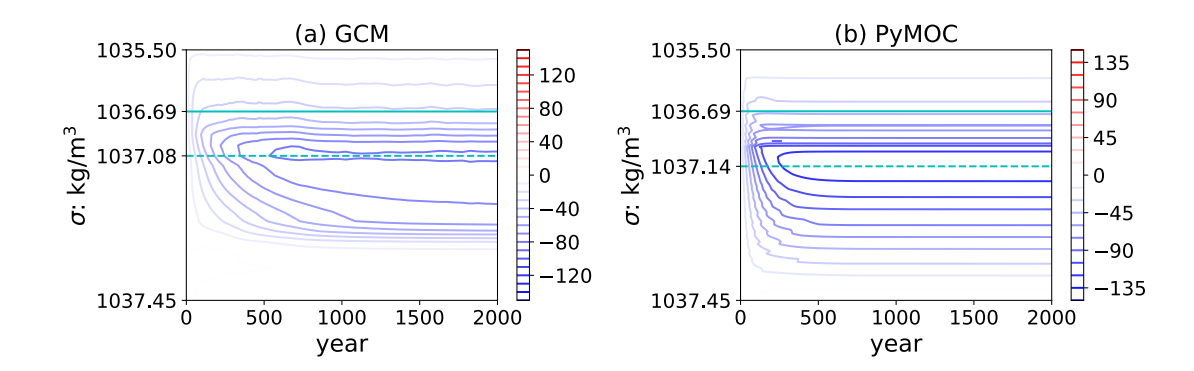


FIG. 8. Hovmöeller diagrams of the isopycnal interface height anomaly from (a) the GCM and (b) PyMOC, in response to an increase in the peak wind stress from  $\tau_0 = 0.2$  Pa to  $\tau_0 = 0.3$  Pa. In the GCM, the interface height is averaged between 40°S and 40°N and excluding the 5° bordering the eastern & western boundaries, consistent with the computation of the pycnocline depth. Negative values denote a deepening of the isopycnals. Notice that the contour interval is 10 m for the GCM and 15 m for PyMOC. The solid cyan lines denote the isopycnal of the MOC maximum, and the dashed cyan lines denote the bottom isopycnal of the MOC.

Two factors appear to determine the adjustment timescale of the pycnocline depth. One is vertical resolution, which needs to be able to represent the depth-dependent adjustment of ocean stratification, shown in Fig. 8. While the isopycnals in the upper ocean adjust on a multi-decadal timescale, the deep isopycnals can take over a thousand years to fully equilibrate, due to the long timescale of diffusion, which approximately scales with the square of the isopycnal depth (cf. Marshall and Zanna 2014). This depth-dependence of the adjustment timescale cannot be captured by the two-layer theory, which has only one (relatively small) depth scale, thus adjusting much faster. The effect of fully resolved vertical stratification is most clearly isolated by comparing PyMOC-no-meander vs. the two-layer theory with n = 8 (Fig. 7(b)(c)), which use similar representations for the eddy-induced MOC in the SO and effectively only differ in their vertical resolutions. The timescale for the pycnocline depth adjustment in PyMOC-no-meander is more than twice as long as in the two-layer theory with n = 8.

The other important factor that determines the adjustment timescale of the pycnocline depth is the sensitivity of the eddy diffusivity to the pycnocline depth, quantified in PyMOC and the two-layer theory via the parameter n. The effect of varying n can be isolated cleanly in the two-layer theory (see Eq. (B3)), and explains the timescale difference between the two versions of the

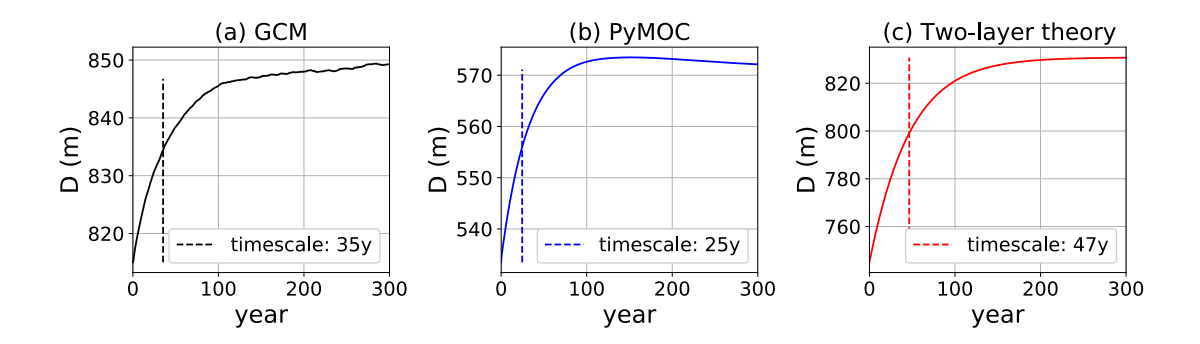


Fig. 9. Time-dependent response of the  $\sigma$  =1036.59 kg m<sup>-3</sup> isopycnal depth, which is at the maximum of the MOC in the reference state, to an increase in the peak wind stress from  $\tau_0$  = 0.2 Pa to  $\tau_0$  = 0.3 Pa, for (a) the GCM and (b) PyMOC. (c) Time-dependent response of the pycnocline depth in the two-layer theory, with n = 3. Corresponding e-folding timescales are listed in legends and indicated by vertical dashed lines.

two-layer theory with n = 3 and 8 (Fig. 7(c)). The same effect also qualitatively explains the slower adjustment in PyMOC (which uses n = 3) compared to PyMOC-no-meander (which uses n = 8).

We can largely eliminate the first factor (the effect of vertical resolution), and hence reconcile the timescale distinction between the GCM/PyMOC and the two-layer theory with n = 3, by interpreting the "pycnocline depth" in the two-layer theory as the depth of a specific isopycnal at the maximum of the MOC. Specifically, if we define the pycnocline depth as the depth of the  $\sigma = 1036.69$  kg m<sup>-3</sup> isopycnal, which is near the depth of both the SOMOC and AMOC maximum in the reference climates of the GCM and PyMOC, all three models indicate roughly similar pycnocline adjustment timescales (Fig. 9). Indeed, this interpretation arguably aligns better with the nature of the two-layer box model, where the "pycnocline depth" serves as the boundary between the upper and lower branches of the AMOC.

# 2) MOC

In the GCM, the MOC adjusts very fast to the wind stress change compared to the pycnocline depth, equilibrating within a few decades (Fig. 10(a)(b)). The SOMOC shows a sudden initial strengthening, which appears to be instantaneous within the 10-year resolution of our data. This initial peak is associated with a slight overshoot that gradually decays to approach the equilibrium value in a few decades. The overshoot is caused by the fast response of the Ekman transport. Meanwhile, baroclinicity, and hence transient eddy transport, is modulated by both the stationary meanders and the stratification in the basin, and we hypothesize that the latter contributes to the

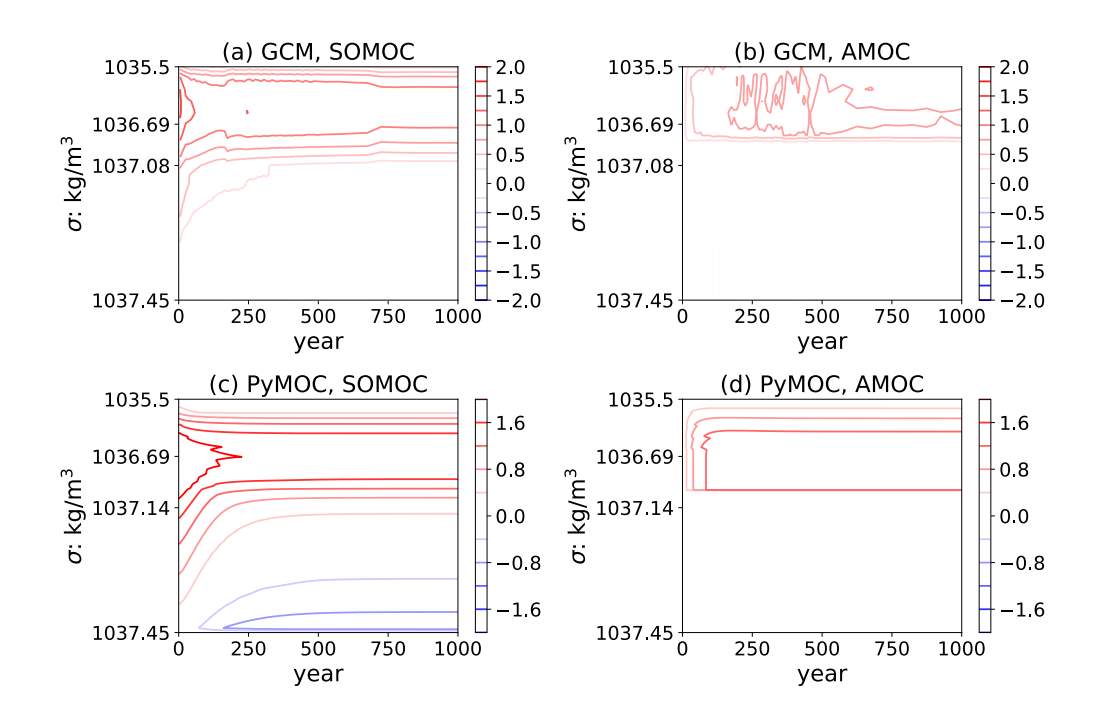


FIG. 10. Hovmöeller diagrams of the SOMOC (left) and AMOC (right) anomaly in the GCM (upper panels) and PyMOC (lower panels) in response to an increase in the peak wind stress from  $\tau_0 = 0.2$  Pa to  $\tau_0 = 0.3$  Pa. For the GCM, the plot is based on 10-year averages for the first 500 years, after which 50-year averages are used. The PyMOC results are based on 10-year averages. The contour interval is 0.25 Sv for the GCM and 0.4 Sv for PyMOC, to account for the generally higher sensitivity in PyMOC, which has previously been shown in Fig. 6. slower SOMOC equilibration after the initial overshoot. By comparison, no significant overshoot is observed in the AMOC response, which approaches its equilibrium value largely monotonically also on a multi-decadal timescale.

The time-dependent MOC response is qualitatively captured by PyMOC (Fig. 10(c)(d))<sup>5</sup>, and the multi-decadal adjustment timescale is also consistent with the two-layer theory, where all circulation components (except for the Ekman transport) adjust on the same multi-decadal timescale as the pycnocline depth (Fig. 7(c)). For the SOMOC, all simple models capture the initial overshoot, followed by a multi-decadal weakening, but they all overestimate the magnitude of the initial overshoot (Fig. 11). In the two-layer theory and PyMOC-no-meander, the large initial overshoot reflects the full response of the Ekman-driven transport, because their eddy-induced MOC is only a

<sup>&</sup>lt;sup>5</sup>Notice that there is a slight negative SOMOC response in the abyssal ocean in PyMOC (Fig. 10(c)). This disagreement with the GCM is likely associated with the presence of topography in the GCM, which generates spatial variations in the isopycnal slope and geostrophic flow below the depth of Scotia Arc, neither of which can be captured in PyMOC, which therefore cannot provide an accurate representation of the abyssal cell (Kong and Jansen 2021; Chang and Jansen 2021). The wind stress response of the abyssal overturning, which is absent in the two-layer theory and poorly represented in PyMOC, is beyond the scope of this paper.

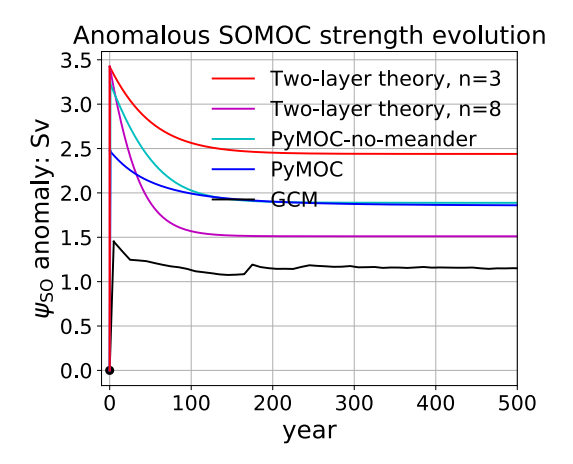


Fig. 11. Time-dependent response of the SOMOC transport to a wind stress increase from  $\tau_0 = 0.2$  Pa to  $\tau_0 = 0.3$  Pa in different models. In the GCM, PyMOC, and PyMOC-no-meander, the SOMOC transport is evaluated at the same isopycnal where the SOMOC maximizes in the reference state:  $\sigma$ =1036.69 kg m<sup>-3</sup>. Notice that the GCM timeseries is based on 10-year averages, and that the Ekman transport, by construction, adjusts instantly to an increase in wind stress in PyMOC and the two-layer model.

function of the stratification in the basin, which equilibrates more slowly. By comparison, PyMOC shows a diminished initial overshoot (albeit still larger than in the GCM), due to the incorporation of the effect of stationary eddies via the stretching factor (Eq. (16)), which implies a rapid response of the eddy transport to wind stress changes, consistent with the GCM simulations. This again highlights the importance of stationary eddies in the transient response of the SO circulation. In the north Atlantic, both PyMOC and the two-layer theory predict a roughly exponential adjustment of the AMOC with a multi-decadal e-folding timescale, consistent with the GCM but much longer than the pycnocline adjustment in both the GCM and PyMOC.

## 3) RELATIONSHIP BETWEEN THE PYCNOCLINE DEPTH AND AMOC

We have shown that the adjustment timescales of the pycnocline depth and AMOC differ significantly, suggesting that their time-dependent relationship also changes with time. This is illustrated in Fig. 12, which shows that the AMOC responds much faster than the pycnocline depth in the first few decades, while the pycnocline depth continues to change after the AMOC has reached equilibrium after several centuries. These disparate responses are captured by PyMOC (Panel (b)); by contrast, the two-layer theory assumes  $T_N \propto D^2$  throughout the adjustment process (black lines in Fig. 12), and thus cannot capture the disparate temporal evolutions of the two quantities.

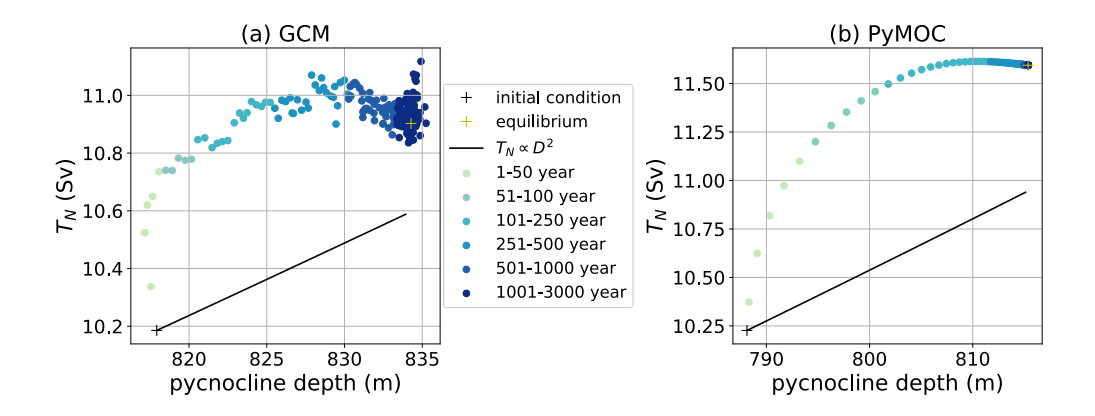


Fig. 12. The temporal relation between the AMOC  $(T_N)$  and pycnocline depth throughout the adjustment process, based on decadal averages, from (a) the GCM and (b) PyMOC. The power-law relation of  $T_N \propto D^2$  is shown as a reference (black lines).

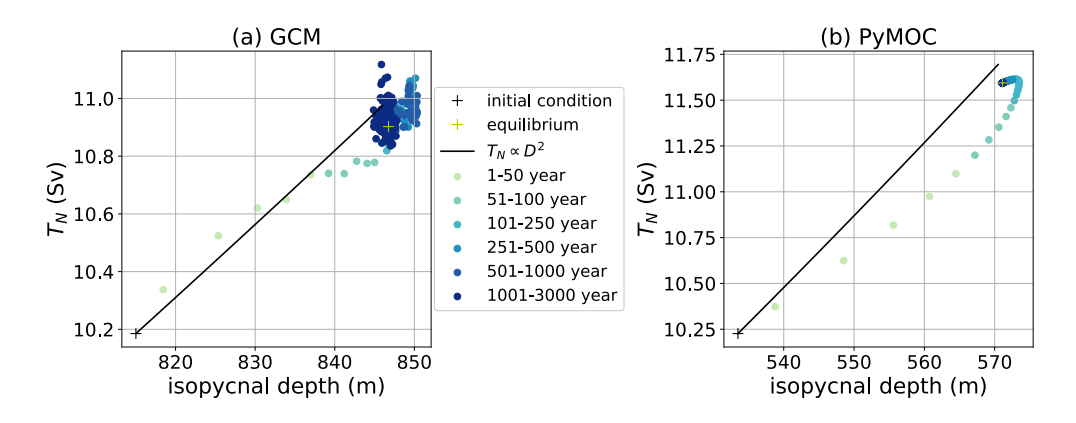


Fig. 13. As in Fig. 12 but for the relation between the AMOC strength and the depth of the  $\sigma = 1036.69 \text{ kg}$  m<sup>-3</sup> isopycnal where the AMOC maximizes.

The reason for the distinct timescales is that while the pycnocline depth adjustment involves the adjustment of stratification throughout the whole depth of the ocean, the AMOC adjustment seems to mostly depend on the isopycnals within the AMOC itself. The isopycnal at the maximum of the AMOC ( $\sigma = 1036.69 \text{ kg m}^{-3}$ ) reaches its new equilibrium depth within a few decades, while the abyssal isopycnals (below the AMOC) take several centuries to millennia to fully equilibrate. Indeed, the temporal relation between the magnitude of the AMOC and the depth of the 1036.69 kg m<sup>-3</sup> isopycnal follows the power-law relation assumed in the theory relatively well in both the GCM and PyMOC (Fig. 13). This not only supports the result that the adjustment of the AMOC depends primarily on the isopycnals within the depth range of the AMOC, but also reinforces our previous argument that the two-layer theory can be reconciled with the GCM/PyMOC if its "pycnocline"

depth" is interpreted as the isopycnal at the maximum of the AMOC. In this case, Eq. (7) is able to capture both the equilibrium and time-dependent relationships between this depth scale and the AMOC. The relatively weak relationship between the AMOC strength and the pycnocline depth is consistent with the results of de Boer et al. (2010), who argue that the more relevant depth scale for the AMOC is the depth of the AMOC maximum.

Our result that the AMOC adjustment is relatively fast and weakly sensitive to the adjustment of the abyssal isopycnals stands in contrast to Jansen et al. (2018), who find that the AMOC equilibrates over a millennial timescale in response to a surface warming, largely due to the slow adjustment of the abyssal isopycnals. A systematic analysis of what governs the different response timescales for different changes in the boundary conditions is beyond the scope of this study, although we speculate that it is related to the effect of the boundary conditions on AABW properties: while the maximum density of AABW remains approximately fixed in our work due to the use of a fast restoring to a fixed surface buoyancy, Jansen et al. (2018) use a constant buoyancy flux condition around Antarctica and change the surface restoring buoyancy elsewhere, which lead to substantial variations in the density of AABW. This large change in the AABW density has previously been argued to affect the depth of the AMOC (de Boer et al. 2010; Nadeau and Jansen 2020). By contrast, the more moderate changes in the abyssal ocean in our simulations appear to have relatively little effect on the AMOC.

## 4. Conclusions and discussion

In this work we have investigated both the equilibrium and transient responses of the overturning circulation and pycnocline depth to changes in Southern Ocean surface wind stress, using a hierarchy of models. Our GCM yields a reference climate state broadly consistent with observations and previous work. For the equilibrium response, consistent with previous studies, we find that in response to a SO wind stress increase, the pycnocline depth deepens and the MOC increases. The SOMOC response is significantly modulated by both stationary and transient eddies in the SO, and thus much weaker than the change in the Ekman-driven transport. The AMOC also responds to a wind stress change, but with a slightly reduced amplitude compared to the SOMOC. The GCM results are approximately reproduced by the PyMOC multi-column model, although the latter slightly overestimates the sensitivities of both the MOC and the diapycnal upwelling. The

two-layer theory of G99 qualitatively captures the reference state and equilibrium responses of the pycnocline depth and AMOC, but significantly overestimates both the reference magnitude and sensitivity of the SOMOC, while substantially underestimating the magnitude but overestimating the sensitivity of the diapycnal upwelling. We attribute this shortcoming primarily to the fact that the pycnocline depth, as defined in G99, does not adequately capture the depth scale that governs the diffusive upwelling in the low-latitude oceans.

For the time-dependent response, we show that in both the GCM and PyMOC, the MOC adjusts on a multi-decadal timescale while the pycnocline depth adjusts on a multi-centennial timescale. By contrast, the two-layer theory of J11, being a time-dependent extension of the two-layer theory of G99, predicts the pycnocline depth to adjust on the same, multi-decadal, timescale as the MOC. We argue that the timescale distinction arises primarily because the pycnocline depth adjustment involves all isopycnals throughout the depth of the ocean, while the MOC seems to be sensitive mostly to the isopycnals that are within the overturning cell. Having only one depth scale, the two-layer theory by construction cannot represent this distinction. One way to reconcile the theory with the numerical model results is by interpreting the "pycnocline depth" in the two-layer theory as the depth of a specific isopycnal near the maximum of the MOC, rather than using the integral definition of the pycnocline depth suggested by G99 (Eq. (18)). We also show that stationary meanders are crucial in rapidly compensating for much of the abrupt response of the Ekman transport to SO wind stress changes, thus suppressing an initial SOMOC "overshoot" that is seen in the simplified models where the effect of standing meanders is not considered.

One caveat of our conclusions is that we have only considered a single-basin configuration, and it remains open in how far a more realistic, multi-basin setup (e.g., Ferrari et al. 2017) may change our conclusions. Nadeau and Jansen (2020) have shown that in equilibrium, what matters for the structure and magnitude of the AMOC is the total area of the domain and the length of the ACC, with a wider domain leading to a deeper and stronger AMOC, as predicted by the G99 model. Adjusting the basin area and ACC length to more realistic global values in the J11 model has a relatively small effect on the predicted adjustment time scale, but it is not clear whether this prediction remains valid for a more realistic model with multiple connected basins.

Our work has several important takeaways. First, the AMOC responds monotonically and rapidly (within decades) to SO wind stress changes in our simulations, in contrast to the non-

monotonic millennial-timescale adjustment recently found for the AMOC response to surface buoyancy changes. Further research is needed to better understand these distinct timescales of AMOC adjustment. Second, despite its obvious advantage for theoretical model development, a two-layer representation of the deep ocean has significant limitations, especially when examining the time-dependent response, which may differ substantially at different depths of the ocean. Last, stationary eddies are crucial for both the transient and equilibrium responses of the SO circulation to surface wind stress changes, and thus deserve more attention in future work.

Acknowledgments. Computational resources for this project were generously provided by the University of Chicago Research Computing Center. We acknowledge support from the National Science Foundation (NSF) through Awards OCE-1846821and OCE-1912163.

Data availability statement. MOM6 (DOI: 10.5281/zenodo.5519595) and PyMOC (DOI: 10.5281/zenodo.5519641) are open source software packages available at GitHub. The specific GCM configuration files used for the experiments in this study are also available at GitHub (DOI: 10.5281/zenodo.5519688).

## APPENDIX A

# **Tuning model parameters**

# a. Tuning two-layer model parameters

There are 11 parameters in the two-layer model of G99 that need to be determined. 7 of them follow more or less directly from the GCM setup:  $L_x$ ,  $L_y$ ,  $\rho$ , f,  $\kappa_d$ , A, and g', and the remaining 4 parameters are chosen to match different aspects of the GCM simulation, as discussed below: the coefficient c (in Eq. (7)), the power n, the reference diffusivity  $K_0$ , and the reference pycnocline depth  $D_0$  (all in Eq. (4)). c = 0.15 is easily determined by matching Eq. (7) with the diagnosed AMOC strength ( $T_N = 10.2$  Sv) and pycnocline depth (D = 818 m) from the GCM simulation under the reference wind stress of  $\tau_0 = 0.2$  Pa.

 $K_0$ ,  $D_0$ , and n together control the SO eddy diffusivity, and are not mutually independent of each other, but effectively control two degrees of freedom: the magnitude of the diffusivity and its sensitivity to wind stress changes. We here consider n = 3 and n = 8, where n = 3 approximately corresponds to the sensitivity of the parameterized diffusivity on the isopycnal slope in the TMEKE parameterization (Jansen et al. 2015, 2019) and n = 8 corresponds to a very sensitive eddy transport, which empirically leads to a better fit to the GCM simulations (Fig. 6), and is also the largest value of n considered in J11. To determine  $K_0$  and  $D_0$ , we aim to match Eq. (5) with the diagnosed effective diffusivity in the GCM,  $K_{\text{eff}}$ , which is defined in Appendix C of Kong and Jansen (2021) as

$$K_{\text{eff}} \approx \frac{\left\{ K_{\text{GM}} | \nabla_z \overline{b}|^2 \right\}}{\left\{ \left[ \partial_y \overline{b} \right]^2 \right\}},$$
 (A1)

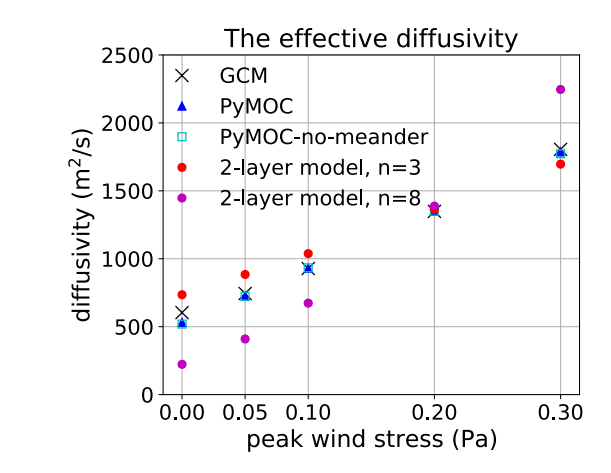


Fig. A1. Diagnosed and parameterized effective diffusivity,  $K_{\text{eff}}$ , from various models. The diffusivity in the GCM is diagnosed as the domain average south of  $40^{\circ}$ S.

where  $\{\cdot\}$  denotes a volume-weighted domain average,  $[\cdot]$  a zonal mean, and  $\overline{(\cdot)}$  a temporal average;  $K_{\text{GM}}$  is the GM diffusivity,  $\nabla_z$  denotes a horizontal gradient, and b is the buoyancy. The averages are based on the domain south of  $40^{\circ}\text{S}$ .

We choose  $K_0 = 1349 \text{ m}^2\text{s}^{-1}$ , which is the diagnosed value of  $K_{\text{eff}}$  in the GCM simulation under the reference wind stress, and  $D_0 = 741 \text{ m}$ , such that  $D = D_0$  under the reference wind stress. This ensures that the choice of n does not influence the results in the reference state, but only controls the sensitivity to wind stress changes. Fig. A1 shows the eddy diffusivity as a function of peak wind stress in comparison with the diagnosed values from the GCM. Notice that the diffusivity with n = 8 appears to be too sensitive to wind stress changes, but this can be attributed to the overly sensitive pycnocline depth (cf. Fig. 6(a)).

## b. Tuning PyMOC parameters

In PyMOC, we largely follow the same procedure as for the two-layer theory to tune the model parameters. As for the two-layer theory, we choose  $D_0$  as the equilibrium value of D under the reference wind stress so that Eq. (16) yields the same diffusivity regardless of n in the reference state. Furthermore, we choose n = 3 since it approximately corresponds to the sensitivity of the diffusivity to isopycnal slope in the TMEKE parameterization (Jansen et al. 2015, 2019). This leaves us to choose  $K_1$  and  $\alpha$  such as to approximately match the magnitude and wind stress

sensitivity of  $K_{\rm eff}$  in the GCM, which yields  $K_1 = 710~{\rm m}^2~{\rm s}^{-1}$  and  $\alpha = 0.9$ . The resulting  $K_{\rm eff}$  almost perfectly matches the diagnosed  $K_{\rm eff}$  in the GCM simulations (Fig. A1).

The parameters for PyMOC-no-meander are chosen following largely the same considerations as used in PyMOC and the two-layer theory. We set  $\alpha = 0$ , which eliminates the explicit parameterization of the stretching effect by standing meanders. The value of  $K_1 = 1349 \text{ m}^2\text{s}^{-1}$  is then again chosen to match  $K_{\text{eff}}$  from the GCM in the reference climate. We further set n=8, which (in equilibrium) leads to virtually the same response of the eddy diffusivity to wind stress changes as in PyMOC, but without explicitly accounting for the wind stress dependence of the standing eddy response (Fig. A1).

Finally, the surface buoyancy in the NADW formation region in both PyMOC and PyMOC-nomeander,  $b_n = 0.004 \text{ ms}^{-2}$ , is chosen to approximately match the surface buoyancy in the northern convection region in the GCM, and the basin "surface buoyancy" (more appropriately interpreted as the buoyancy below the ventilated thermocline)  $b_0 = 0.018 \text{ ms}^{-2}$  is chosen to approximately match the AMOC strength in the reference state of the GCM.

## APPENDIX B

# The adjustment timescale for the pycnocline depth in the two-layer theory

The derivation below was originally presented in Jones (2013), and is here reproduced for completeness. Assuming the change of D is small compared to its equilibrium value  $D_{\rm eq}$ , we can express its time-dependent value as  $D(t) = D_{\rm eq} + \Delta D(t)$ , with  $|\Delta D(t)| \ll |D_{\rm eq}|$ , and substitute into Eq. (8) to obtain

$$A\frac{d\Delta D}{dt} = \frac{\tau L_{x}}{\rho |f|} - \frac{L_{x}K_{0}}{L_{y}D_{0}^{n-1}} (D_{eq} + \Delta D)^{n} + \frac{\kappa_{d}A}{D_{eq} + \Delta D} - \frac{Cg'}{f} (D_{eq} + \Delta D)^{2}$$

$$= T_{Ek,eq} - T_{eddy,eq} \left( 1 + \frac{\Delta D}{D_{eq}} \right)^{n} + T_{U,eq} \left( 1 + \frac{\Delta D}{D_{eq}} \right)^{-1} - T_{N,eq} \left( 1 + \frac{\Delta D}{D_{eq}} \right)^{2}$$

$$\approx T_{Ek,eq} - T_{eddy,eq} \left( 1 + \frac{n\Delta D}{D_{eq}} \right) + T_{U,eq} \left( 1 - \frac{\Delta D}{D_{eq}} \right) - T_{N,eq} \left( 1 + \frac{2\Delta D}{D_{eq}} \right)$$

$$= (T_{Ek,eq} - T_{eddy,eq} + T_{U,eq} - T_{N,eq}) - (nT_{eddy,eq} + T_{U,eq} + 2T_{N,eq}) \frac{\Delta D}{D_{eq}}$$

$$= - (nT_{eddy,eq} + T_{U,eq} + 2T_{N,eq}) \frac{\Delta D}{D_{eq}}, \tag{B1}$$

where we have applied Eq. (1) and discarded the higher order terms. Eq. (B1) can be rewritten as

$$\frac{\mathrm{d}\Delta D}{\mathrm{dt}} = -\frac{T_{\mathrm{U,eq}} + 2T_{\mathrm{N,eq}} + nT_{\mathrm{eddy,eq}}}{AD_{\mathrm{eq}}} \Delta D,$$
(B2)

which can be solved to get

$$\Delta D(t) = \Delta D(t = 0) \exp\left[-t \cdot \frac{T_{\text{U,eq}} + 2T_{\text{N,eq}} + nT_{\text{eddy,eq}}}{AD_{\text{eq}}}\right], \tag{B3}$$

yielding the e-folding adjustment timescale in Eq. (9).

## References

- Abernathey, R., and P. Cessi, 2014: Topographic enhancement of eddy efficiency in baroclinic equilibration. *J. Phys. Oceanogr.*, **44** (**8**), 2107–2126, https://doi.org/10.1175/JPO-D-14-0014.1.
- Abernathey, R., J. Marshall, and D. Ferreira, 2011: The dependence of southern ocean meridional overturning on wind stress. *J. Phys. Oceanogr.*, **41** (**12**), 2261–2278, https://doi.org/10.1175/JPO-D-11-023.1.
- Allison, L., H. Johnson, and D. Marshall, 2011: Spin-up and adjustment of the antarctic circumpolar current and global pycnocline. *J. Mar. Res.*, **69**, 167–189, https://doi.org/10.1357/002224011798765330.
- Chang, C.-Y., and M. F. Jansen, 2021: Distinct controls on the strength of the abyssal overturning circulation: Channel versus basin dynamics. *Journal of Physical Oceanography*, **51** (**7**), 2073 2086, https://doi.org/10.1175/JPO-D-20-0316.1.
- de Boer, A. M., A. Gnanadesikan, N. R. Edwards, and A. J. Watson, 2010: Meridional density gradients do not control the atlantic overturning circulation. *Journal of Physical Oceanography*, **40** (2), 368 380, https://doi.org/10.1175/2009JPO4200.1.
- Delworth, T. L., and F. Zeng, 2008: Simulated impact of altered southern hemisphere winds on the atlantic meridional overturning circulation. *Geophysical Research Letters*, **35** (**20**), https://doi.org/10.1029/2008GL035166.

- Farneti, R., and T. L. Delworth, 2010: The role of mesoscale eddies in the remote oceanic response to altered southern hemisphere winds. *Journal of Physical Oceanography*, **40** (**10**), 2348 2354, https://doi.org/10.1175/2010JPO4480.1.
- Ferrari, R., L.-P. Nadeau, D. P. Marshall, L. C. Allison, and H. L. Johnson, 2017: A model of the ocean overturning circulation with two closed basins and a reentrant channel. *Journal of Physical Oceanography*, **47** (**12**), 2887 2906, https://doi.org/10.1175/JPO-D-16-0223.1, URL https://journals.ametsoc.org/view/journals/phoc/47/12/jpo-d-16-0223.1.xml.
- Fürst, J. J., and A. Levermann, 2012: A minimal model for wind- and mixing-driven overturning: threshold behavior for both driving mechanisms. *Climate Dynamics*, **38**, 239–260, https://doi.org/10.1007/s00382-011-1003-7.
- Gent, P. R., and J. C. McWilliams, 1990: Isopycnal mixing in ocean circulation models. *J. Phys. Oceanogr.*, **20** (**1**), 150–155, https://doi.org/10.1175/1520-0485(1990)020<0150:IMIOCM>2. 0.CO;2.
- Gnanadesikan, A., 1999: A simple predictive model for the structure of the oceanic pycnocline. *Science*, **283** (**5410**), 2077–2079, https://doi.org/10.1126/science.283.5410.2077.
- Hallberg, R., and A. Gnanadesikan, 2006: The role of eddies in determining the structure and response of the wind-driven southern hemisphere overturning: Results from the modeling eddies in the southern ocean (meso) project. *J. Phys. Oceanogr.*, **36** (**12**), 2232–2252, https://doi.org/10.1175/JPO2980.1.
- Jansen, M. F., A. Adcroft, S. Khani, and H. Kong, 2019: Toward an energetically consistent, resolution aware parameterization of ocean mesoscale eddies. *J. Adv. Model. Earth Sys.*, **11 (8)**, 2844–2860, https://doi.org/10.1029/2019MS001750.
- Jansen, M. F., A. J. Adcroft, R. Hallberg, and I. M. Held, 2015: Parameterization of eddy fluxes based on a mesoscale energy budget. *Ocean Model.*, **92**, 28 41, https://doi.org/https://doi.org/10.1016/j.ocemod.2015.05.007.
- Jansen, M. F., and L.-P. Nadeau, 2019: A toy model for the response of the residual overturning circulation to surface warming. *Journal of Physical Oceanography*, **49** (5), 1249

- 1268, https://doi.org/10.1175/JPO-D-18-0187.1, URL https://journals.ametsoc.org/view/journals/phoc/49/5/jpo-d-18-0187.1.xml.
- Jansen, M. F., L.-P. Nadeau, and T. M. Merlis, 2018: Transient versus equilibrium response of the ocean's overturning circulation to warming. *J. Climate*, 31 (13), 5147–5163, https://doi.org/ 10.1175/JCLI-D-17-0797.1.
- Jones, D. C., 2013: Testing eddy compensation and eddy saturation in the southern ocean. *PhD dissertation*, URL http://hdl.handle.net/10217/79441.
- Jones, D. C., T. Ito, and N. S. Lovenduski, 2011: The transient response of the southern ocean pycnocline to changing atmospheric winds. *Geophysical Research Letters*, **38** (**15**), https://doi.org/10.1029/2011GL048145.
- Klinger, B. A., and C. Cruz, 2009: Decadal response of global circulation to southern ocean zonal wind stress perturbation. *Journal of Physical Oceanography*, **39** (8), 1888 1904, https://doi.org/10.1175/2009JPO4070.1.
- Kong, H., and M. F. Jansen, 2021: The impact of topography and eddy parameterization on the simulated southern ocean circulation response to changes in surface wind stress. *Journal of Physical Oceanography*, **51** (3), 825 843, https://doi.org/10.1175/JPO-D-20-0142.1.
- Lumpkin, R., and K. Speer, 2007: Global Ocean Meridional Overturning. *Journal of Physical Oceanography*, **37** (**10**), 2550–2562, https://doi.org/10.1175/JPO3130.1.
- Ma, H., L. Wu, and C. Li, 2010: The role of southern high latitude wind stress in global climate. *Advances in Atmospheric Sciences*, **27**, 371–381, https://doi.org/10.1007/s00376-009-9047-x.
- Mak, J., J. R. Maddison, D. P. Marshall, and D. R. Munday, 2018: Implementation of a geometrically informed and energetically constrained mesoscale eddy parameterization in an ocean circulation model. *J. Phys. Oceanogr.*, **48** (**10**), 2363–2382, https://doi.org/10.1175/JPO-D-18-0017.1.
- Marshall, D., and L. Zanna, 2014: A conceptual model of ocean heat uptake under climate change. *Journal of Climate*, **27** (**22**), 8444–8465, https://doi.org/10.1175/JCLI-D-13-00344.1, publisher

- Copyright: © 2014 American Meteorological Society. Copyright: Copyright 2018 Elsevier B.V., All rights reserved.
- Marshall, J., and T. Radko, 2003: Residual-mean solutions for the antarctic circumpolar current and its associated overturning circulation. *J. Phys. Oceanogr.*, **33** (**11**), 2341–2354, https://doi.org/10.1175/1520-0485(2003)033<2341:RSFTAC>2.0.CO;2.
- Marshall, J., and K. Speer, 2012: Closure of the meridional overturning circulation through southern ocean upwelling. *Nature Geoscience*, **5**, 171–180, https://doi.org/10.1038/ngeo1391.
- Morrison, A. K., and A. M. Hogg, 2013: On the relationship between southern ocean overturning and acc transport. *J. Phys. Oceanogr.*, **43** (1), 140–148, https://doi.org/10.1175/JPO-D-12-057.1.
- Munday, D. R., H. L. Johnson, and D. P. Marshall, 2013: Eddy saturation of equilibrated circumpolar currents. *J. Phys. Oceanogr.*, **43** (3), 507–532, https://doi.org/10.1175/JPO-D-12-095.1.
- Nadeau, L.-P., and M. F. Jansen, 2020: Overturning circulation pathways in a two-basin ocean model. *Journal of Physical Oceanography*, **50** (8), 2105 2122, https://doi.org/10.1175/JPO-D-20-0034.1.
- Nakamura, N., 1996: Two-dimensional mixing, edge formation, and permeability diagnosed in an area coordinate. *J. Atmos. Sci.*, **53** (**11**), 1524–1537, https://doi.org/10.1175/1520-0469(1996) 053<1524:TDMEFA>2.0.CO;2.
- Nakamura, N., 2001: A new look at eddy diffusivity as a mixing diagnostic. *J. Atmos. Sci.*, **58 (24)**, 3685–3701, https://doi.org/10.1175/1520-0469(2001)058<3685:ANLAED>2.0.CO;2.
- Nikurashin, M., and G. Vallis, 2011: A Theory of Deep Stratification and Overturning Circulation in the Ocean. *Journal of Physical Oceanography*, **41** (3), 485–502, https://doi.org/10.1175/2010JPO4529.1.
- Nikurashin, M., and G. Vallis, 2012: A theory of the interhemispheric meridional overturning circulation and associated stratification. *J. Phys. Oceanogr.*, **42** (**10**), 1652–1667, https://doi.org/10.1175/JPO-D-11-0189.1.

- Samelson, R. M., 2011: Time-Dependent Adjustment in a Simple Model of the Mid-Depth Meridional Overturning Cell. *Journal of Physical Oceanography*, **41** (**5**), 1009–1025, https://doi.org/10.1175/2010JPO4562.1.
- Sévellec, F., and A. V. Fedorov, 2011: Stability of the atlantic meridional overturning circulation and stratification in a zonally averaged ocean model: Effects of freshwater flux, southern ocean winds, and diapycnal diffusion. *Deep Sea Research Part II: Topical Studies in Oceanog-raphy*, **58** (**17**), 1927–1943, https://doi.org/10.1016/j.dsr2.2010.10.070, climate and the Atlantic Meridional Overturning Circulation.
- Shakespeare, C. J., and A. M. Hogg, 2012: An analytical model of the response of the meridional overturning circulation to changes in wind and buoyancy forcing. *Journal of Physical Oceanography*, **42** (**8**), 1270 1287, https://doi.org/10.1175/JPO-D-11-0198.1.
- Sinha, A., and R. P. Abernathey, 2016: Time scales of southern ocean eddy equilibration. *J. Phys. Oceanogr.*, **46** (**9**), 2785–2805, https://doi.org/10.1175/JPO-D-16-0041.1.
- Thompson, A. F., and A. C. Naveira Garabato, 2014: Equilibration of the antarctic circumpolar current by standing meanders. *J. Phys. Oceanogr.*, **44** (7), 1811–1828, https://doi.org/10.1175/JPO-D-13-0163.1.
- Toggweiler, J., and B. Samuels, 1995: Effect of drake passage on the global thermohaline circulation. *Deep Sea Research Part I: Oceanographic Research Papers*, **42** (**4**), 477–500, https://doi.org/10.1016/0967-0637(95)00012-U.
- Viebahn, J., and C. Eden, 2010: Towards the impact of eddies on the response of the southern ocean to climate change. *Ocean Model.*, **34**, 150–165, https://doi.org/10.1016/j.ocemod.2010.05.005.
- Visbeck, M., J. Marshall, T. Haine, and M. Spall, 1997: Specification of eddy transfer coefficients in coarse-resolution ocean circulation models. *J. Phys. Oceanogr.*, **27** (**3**), 381–402, https://doi.org/10.1175/1520-0485(1997)027<0381:SOETCI>2.0.CO;2.
- Wearn, R. B., and D. Baker, 1980: Bottom pressure measurements across the antarctic circumpolar current and their relation to the wind. *Deep Sea Research Part A. Oceanographic Research Papers*, **27** (**11**), 875–888, https://doi.org/https://doi.org/10.1016/0198-0149(80)90001-1.

- Wei, W., G. Lohmann, and M. Dima, 2012: Distinct modes of internal variability in the global meridional overturning circulation associated with the southern hemisphere westerly winds. *Journal of Physical Oceanography*, **42** (**5**), 785 – 801, https://doi.org/10.1175/JPO-D-11-038.1.
- Wolfe, C. L., and P. Cessi, 2011: The adiabatic pole-to-pole overturning circulation. *Journal of Physical Oceanography*, **41** (**9**), 1795 1810, https://doi.org/10.1175/2011JPO4570.1.